Strong magnetoelastic coupling in orthorhombic $Eu_{1-x}Y_xMnO_3$ manganite

J. Agostinho Moreira,* A. Almeida, W. S. Ferreira, J. P. Araújo, A. M. Pereira, and M. R. Chaves
IFIMUP and IN-Institute of Nanoscience and Nanotechnology, Departamento de Física e Astronomia da Faculdade de Ciências, Universidade do Porto, Rua do Campo Alegre 687, 4169-007 Porto, Portugal

M. M. R. Costa and V. A. Khomchenko
Centro de Estudos de Materiais por Difracção de Raios-X, Departamento de Física da Faculdade de Ciências e Tecnologia, Universidade de Coimbra, Rua Larga, 3004-516 Coimbra, Portugal

J. Kreisel
Laboratoire des Matériaux et du Génie Physique, MINATEC, Grenoble Institute of Technology, CNRS, 38016 Grenoble, France

D. Chernyshov
Swiss-Norwegian Beam Lines, European Synchrotron Radiation Facility (ESRF), 38000 Grenoble, France

S. M. F. Vilela and P. B. Tavares
Centro de Química-Vila Real, Universidade de Trás-os-Montes e Alto Douro, Apartado 1013, 5001-801 Vila Real, Portugal
(Received 26 May 2010; published 10 September 2010)

This work reports an experimental study on the temperature dependence of the structural parameters in orthorhombic $Eu_{1-x}Y_xMnO_3$ system at low temperatures, by using synchrotron x-ray diffraction technique. A significant magnetoelastic coupling is revealed by anomalies observed in lattice parameters at the magnetic phase transitions, apparent also in both Mn-O bond lengths and Mn-O1-Mn bond angle. Furthermore, signatures of the lattice deformations across the magnetic phase transitions were evidenced by anomalies in the temperature dependence of the lattice mode involving rotations of the MnO_6 octahedra. These anomalies confirm the important role of the spin-phonon coupling in these materials.

DOI: 10.1103/PhysRevB.82.094418 PACS number(s): 75.47.Lx, 61.05.cp, 77.80.−e, 77.22.Ej

I. INTRODUCTION

Magnetoelectric compounds have attracted a lot of interest in the scientific community due to the coupling between electric polarization and magnetic order.[1–4] Particularly, multiferroic materials, which exhibit ferromagnetism and ferroelectricity coupled together in the same thermodynamic phase, are of considerable interest due to their potential applicability in technological devices, opening the possibility to control spin transport electrically.[5,6] In earlier published works, it has been evidenced that the mechanisms underlying magnetoelectricity and multiferroicity are complex, involving both competitive magnetic interactions and spin-phonon coupling.[7–10] Despite the intensive experimental studies performed in several families of magnetoelectric compounds, no universal model was proposed. In fact, it has been assumed that the inverse Dzyaloshinskii-Moriya interaction induces the electric polarization of the electronic orbitals, without the involvement of the lattice degrees of freedom.[11] An alternative model was proposed in Ref. 12, which states that the Dzyaloshinskii-Moriya interaction has two different effects: it induces the ferroelectric state through lattice deformations and stabilizes the magnetic structure at low temperatures.

Among rare-earth manganites, orthorhombic $GdMnO_3$, $TbMnO_3$, and $DyMnO_3$ have shown magnetoelectric properties.[13] The sinusoidal antiferromagnetic (AFM) order in $TbMnO_3$ and $DyMnO_3$ is considered to be responsible for the modulation of the Mn-O1-Mn angle, which has been taken as primary order parameter in these improper ferroelectrics.[7] Goto *et al.*[7] have stressed the importance of the Mn-O1-Mn bond angle conditioning the orbital overlapping and, thus, underlying the physical properties of the phase sequences at low temperatures. It has been found that the superexchange integrals of nearest-neighbor (NN) ferromagnetic ($J_1<0$) and next-nearest-neighbor (NNN) antiferromagnetic ($J_2>0$) interactions between the Mn spins depend strongly on the Mn-O1-Mn angle.[7] Namely, it has been shown that with decreasing the Mn-O1-Mn bond angle, $|J_1|$ decreases and $|J_2|$ increases, due to a large overlap integral between the two oxygen $2p$ orbitals along the $a+b$ axis.[7] Therefore, the system is regarded as a frustrated spin system described by the so-called J_1-J_2 localized spin model. The systematic change in magnetic ordering induced by a change in the rare-earth ion in $RMnO_3$ is understood by the frustrated model; the A-type antiferromagnetic order arises mainly from the NNN antiferromagnetic interaction J_2. Later, Dong *et al.*[14] have described the stabilization of the spiral phase in rare-earth manganites by considering a relatively weak next-nearest-neighbor superexchange coupling and the Jahn-Teller distortion.

In the magnetically driven ferroelectrics, lattice distortion, owing to the coupling with magnetic momenta, has been considered to be the very origin of the spontaneous polarization apparent in the temperature range of stability of the ferroelectric phase. Attempts have been undertaken to establish the order of magnitude of those distortions, but one major handicap has been their small size, which is expected to be three or more orders of magnitude lower than that of typical ferroelectrics like $BaTiO_3$.[15–18] Surprisingly though, recently published results for the hexagonal $YMnO_3$ and

$LuMnO_3$ showed unusual large displacements near T_N, giving rise to a giant magnetoelastic coupling in these materials.[19] Yet, the ferroelectric polarization remains almost constant through T_N. Unlike the usual ferroelectrics, the isostructural transition of the referred hexagonal compounds at T_N is not accompanied by a soft mode.

A detailed and systematic experimental study of the mechanisms associated with the coupling between magnetic order and electric polarization in rare-earth manganites is still missing. The aforementioned $GdMnO_3$, $TbMnO_3$, and $DyMnO_3$ compounds are not the best candidates for such a study because changes on the Mn-O1-Mn angle are also affected by changes on the magnetic momenta of the unit cell whenever a rare-earth ion is replaced by another. On the other hand, the possibility of systematic and fine tuning of the *A*-site size, without increasing the magnetic complexity arising from the rare-earth ion, can be achieved by the isovalent substitution of the trivalent Eu^{3+} ion by Y^{3+} in $Eu_{1-x}Y_xMnO_3$, for $x<0.55$. For this system a continuous variation in the Mn-O1-Mn bond angle is expected, which is associated with the development of the complex magnetic ground states and ferroelectric phases, analogous to the nondoped $GdMnO_3$, $TbMnO_3$, and $DyMnO_3$.

Earlier literature reports on $Eu_{1-x}Y_xMnO_3$, with $0\leq x<0.55$, have already shown that this system exhibits a complex and interesting phase diagram with various magnetic and ferroelectric phases, making it an attractive system to study coupling between polar, magnetic, and structural degrees of freedom.[20–24] Notwithstanding numerous studies, the phase diagram is still not unambiguously established (see Sec. II for more details). Moreover, despite the observation of spin-phonon coupling and the existence of electromagnons in $Eu_{1-x}Y_xMnO_3$, evidenced through both Raman-scattering and infrared spectroscopies,[21,25–28] no information has yet been reported regarding the lattice deformations occurring across the low-temperature magnetic phase transitions, as well as their contribution to the spin-lattice coupling. The emergence of an electric polarization implies a loss of the inversion symmetry center and lattice deformations, arising from atomic polar displacements. As a consequence, a carefully study of the crystallographic structure across the phase transitions is desirable.

In this paper, we present a detailed study on the temperature dependence of the lattice parameters in orthorhombic $Eu_{1-x}Y_xMnO_3$, in the concentration range $0\leq x\leq 0.4$, by using synchrotron-radiation powder diffraction. We aim at correlating the temperature dependence of lattice distortions with the magnetic phase-transition sequence, and, in this way, getting further information regarding the coupling between the spin system and the lattice, which yields large magnetoelastic coupling in these compounds. Furthermore, signatures of the lattice deformations across the magnetic phase transitions will be searched for in the temperature dependence of lattice modes involving MnO_6 octahedra. These signatures can give most relevant information regarding the role of the spin-phonon coupling in these materials.

II. GENERAL CONSIDERATIONS AND THE PHASE DIAGRAM OF $Eu_{1-x}Y_xMnO_3$, $x<0.55$

In this section, we critically review the literature on the phase diagram of $Eu_{1-x}Y_xMnO_3$, $x<0.55$, as it will be crucial for the understanding of our main outcomes of this work.

$Eu_{1-x}Y_xMnO_3$, with $0\leq x<0.55$, exhibits distinctive features making it an attractive system to study. In this system, physical properties are driven by the magnetic spin of the Mn^{3+} ions, but they can be drastically changed by varying the content of Y^{3+}, which does not carry any magnetic moment but changes the effective *A*-site size, and, thus, the Mn-O1-Mn bond angle.[21] The phase diagram of $Eu_{1-x}Y_xMnO_3$, with $0\leq x<0.55$, has been described on the grounds of competitive NN ferromagnetic and NNN antiferromagnetic interactions, along with single-ion anisotropy and the Dzyaloshinskii-Moriya interaction.[29] As a consequence, these compounds exhibit a rich variety of phase transitions from incommensurate to commensurate antiferromagnetic phases, some of them with a ferroelectric character, depending on the extent of chemical substitution *x*.

Ivanov *et al.*,[22] Hemberger *et al.*,[23] and Yamasaki *et al.*[24] have proposed (x,T) phase diagrams, for $Eu_{1-x}Y_xMnO_3$ single crystals, with $0\leq x<0.55$, obtained by using both identical and complementary experimental techniques. Although the proposed phase diagrams present discrepancies regarding the magnetic phase sequence and the ferroelectric properties for $0.15<x<0.25$, there is a good agreement concerning the phase sequence for $0.25<x<0.55$.

For all compounds, the paramagnetic-paraelectric state above $T_N\approx 50-45$ K, is followed by an ordered antiferromagnetic phase (AFM-1) with incommensurate modulation of the manganese spins. According to Hemberger *et al.*,[23] for $x<0.15$, a weakly ferromagnetic phase is established, with a canted *A*-type antiferromagnetic order (AFM-3). On the other hand, Yamasaki *et al.*[24] have reported the spread of this phase over *x* up to 0.25. Due to the collinear structure, this antiferromagnetic phase is not ferroelectric in the absence of an applied magnetic field. Very recently, Tokunaga *et al.*[30] have published a high magnetic field study of the polar properties of $EuMnO_3$ and $Eu_{0.9}Y_{0.1}MnO_3$. Application of magnetic fields parallel to the *b* axis, as high as 20 T, causes first-order transition to the ferroelectric phase, with polarization parallel to the *a* axis, below 44 K.

For higher concentrations $x>0.25$, the ground state is antiferromagnetic (AFM-2) and ferroelectric, without a ferromagnetic component.[23,24] The modulation vector $(0\ q_l\ 0)$ persists down to 5 K, and the magnetic structure is cycloidal.[24] For $x>0.35$, two successive ferroelectric phase transitions occur, with spontaneous polarization along the *c* axis and *a* axis, respectively.[23,24] In agreement with the inverse Dzyaloshinskii-Moriya model, the direction of the electric polarization is associated with the *bc*- and *ab*-cycloidal states, which can be reversed by an applied magnetic field.[31] In these ferroelectric phases, a remarkable magnetic anisotropy is found. A microscopic model has shown that the Dzyaloshinskii-Moriya interaction between spins neighboring along the cubic *x* and *y* axes, as well as, the single-ion anisotropy favor the *ab*-cycloidal spin state with $P\|a$ while the Dzyaloshinskii-Moriya interactions between spins neighboring along the *c* axis favor the *bc*-cycloidal state with $P\|c$. Their competition is controlled by the NNN J_2 exchanges enhanced by lattice distortion, This leads to a lattice-distortion-induced reorientation of polarization from *c* to *a* with decreasing the *A*-site radius.[29]

The phase diagram of the range of compositions $0.15 < x < 0.25$ is still controversial. For the special case of $x = 0.20$, Hemberger *et al.*[23] detected in both specific heat and electric permittivity hints for another phase transition at $T_{AFM\text{-}2} = 30$ K. Double magnetic hysteresis loops at 25 K were reported, revealing the antiferromagnetic character of the phase below $T_{AFM\text{-}2}$.[23] Based on the anomalous behavior observed in the electric permittivity and magnetization curves, a canted antiferromagnetic phase (AFM-3) below $T_{AFM\text{-}3} = 22$ K was proposed.[23] According to Hemberger *et al.*,[23] $Eu_{0.8}Y_{0.2}MnO_3$ becomes ferroelectric below $T_{AFM\text{-}2} = 30$ K along the *a* direction. The ferroelectric character of both low-temperature AFM-2 and AFM-3 magnetic phases was also found by Valdés *et al.* in $Eu_{0.75}Y_{0.25}MnO_3$.[26] Taking into account the weak ferromagnetic character of the AFM-3 phase, as well as the electric polarization below $T_{AFM\text{-}2} = 30$ K, Hemberger *et al.*[23] have proposed a noncollinear spiral order for the AFM-2 phase, and a spin-canting conelike structure, for the AFM-3 one. The actual magnetic ordering of the low-temperature phases, however, remains still unknown. On the other hand, Yamasaki *et al.*[24] have reported another phase sequence for $Eu_{0.8}Y_{0.2}MnO_3$ from the incommensurate magnetic phase to the canted *A*-type antiferromagnetic one (AFM-2), without any ferroelectric properties. Very recently, a carefully study of the $P(E)$ hysteresis loops and pyroelectric current has shown that the ferroelectric character of the $Eu_{0.8}Y_{0.2}MnO_3$ only appears between $T_{AFM\text{-}2}$ and $T_{AFM\text{-}3}$; i.e., in the AFM-2 phase, with very small values of the spontaneous polarization, arising from lattice deformations underlined by the microscopic mechanisms associated with the phase transition at $T_{AFM\text{-}2}$.[21,32]

The origin of the ferroelectricity in these compounds could be understood in the framework of the spin-driven ferroelectricity model. In these frustrated spin systems, the inverse Dzyaloshinskii-Moriya interaction mechanism has been proposed.[11] However, based on experimental results, the magnetic structure has been well established only for the compositions $x = 0.4$ and 0.5. For the other compositions, the magnetic structure is not yet elucidated.

The ferroelectric properties of the $Eu_{1-x}Y_xMnO_3$ have also been studied by measurement of the electric current after cooling the sample under rather high-applied electric fields ($E > 1$ kV/cm). As it was shown in Refs. 32 and 33, $Eu_{1-x}Y_xMnO_3$ exhibits a rather high polarizability, which can hinder the actual spontaneous polarization to be ascertained. In this case, a special experimental procedure has to be carried out.[32,33]

III. EXPERIMENTAL

High-quality $Eu_{1-x}Y_xMnO_3$ ceramics were prepared by the sol-gel urea combustion method. A detailed study of $EuMnO_3$ and $GdMnO_3$ ceramics prepared in this way has led to results very similar to the ones obtained in the corresponding single crystals.[20]

The valence of the europium ion was checked through x-ray photoemission spectroscopy technique, and no evidences of the existence of valences other than the Eu (III) could be detected. As the samples were fast cooled from 1350 °C down to room temperature, significant deviations of the oxygen occupancy from the expected stoichiometric $Eu_{0.8}Y_{0.2}MnO_3$ are not expected, thus excluding the existence of significant amount of Mn (IV) ion.[34] The Rietveld refinement of powder x-ray diffraction data revealed no impurity phases. Refined occupancies of crystallographic positions were found to correspond to the nominal compositions of the samples.

The dielectric and magnetic properties of all samples prepared were previously studied and compared with published data.[21,33,35] No significant differences between the temperature dependence of the dielectric constant and of the specific-induced magnetization obtained in this work and those published in current literature were detected. These results, along with the data obtained from the x-ray diffraction and energy dispersion spectroscopy attest the high quality of our samples.

Synchrotron x-ray diffraction experiments were performed at the beamline BM01A (Swiss-Norwegian Beamlines) at the European Synchrotron Radiation Facility (ESRF), Grenoble, France. For each composition, a powder sample prepared with uniform grain size was enclosed in a sealed Lindemann glass capillary (0.2 mm diameter to minimize the absorption factor, $\rho \cdot \mu \cdot r$ and 0.01 mm wall thickness) and mounted on an appropriate golden plate sample holder to be attached to the cryostat.

Diffraction data were collected using a wavelength of $\lambda = 0.70$ Å from a Si(111) double crystal monochromator and a MAR345 image plate detector at a sample-to-detector distance of 220 mm. This setup was found to be a good compromise between resolution and accessible range of *d* spacing. Calibration was performed by using a LaB_6 powder as a reference material (NIST standard reference material 660a). The powder sample remained stationary during data collection. The exposure times for each data set were selected between 10 and 20 s to avoid oversaturation of the detector. Measurements were made at temperatures between 5 and 290 K. The samples were cooled in a flow He cryostat.

Preliminary data reduction, including reconstruction of two-dimensional diffraction patterns from the raw data, was carried out using the ESRF FIT2D software,[36] yielding intensity versus 2θ diffraction pattern. Calculation of standard deviations and scaling of different data was done with a locally developed software. The x-ray patterns were analyzed with reasonable agreement factor using the FULLPROF software.[37]

IV. EXPERIMENTAL RESULTS AND DISCUSSION

A. Structural refinement

The powder x-ray diffraction patterns obtained for the $Eu_{1-x}Y_xMnO_3$ ceramics, with $x = 0$, 0.2, 0.3, and 0.4, investigated in the temperature range 5–300 K, were refined using Rietveld analysis in order to follow the evolution of relevant structural parameters. All patterns revealed the orthorhombic structure *Pbnm* above T_N. A typical result of this analysis is shown in Fig. 1.

Below or above $T_{AFM\text{-}2}$ the x-ray patterns are qualitatively similar. As an example, Fig. 2 exhibits the x-ray patterns recorded in $Eu_{0.8}Y_{0.2}MnO_3$ at 15 K, 23 K, and 35 K, respec-

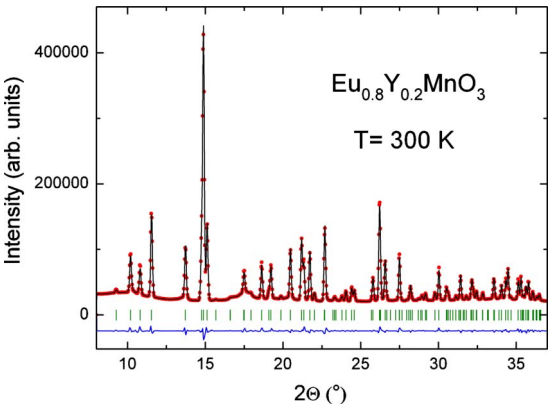

FIG. 1. (Color online) Observed, calculated, and difference x-ray diffraction patterns for the $Eu_{0.8}Y_{0.2}MnO_3$ compound at room temperature.

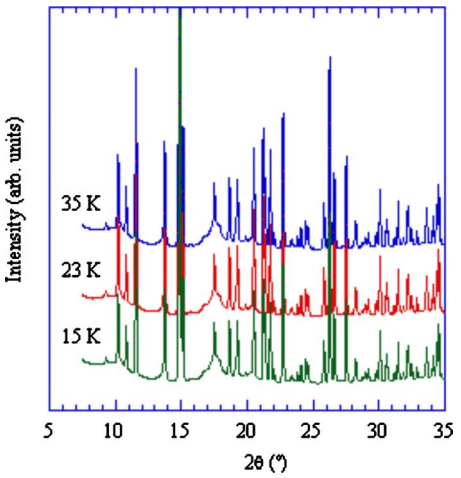

FIG. 2. (Color online) X-ray patterns of $Eu_{0.8}Y_{0.2}MnO_3$ recorded at 15, 23, and 35 K.

tively. No additional reflections could be detected in the ferroelectric phase. Taking into account the value of the remanent polarization presented in Refs. 21, 32, and 33, the average ion displacement is estimated to be about 10^{-5} Å, which is typical for improper ferroelectric phases, as it is the case in rare-earth manganites. No satellites associated with the modulated structure have been detected, as well as peak splitting associated with symmetry reduction. In these conditions, we have no reasons to use a space group different from *Pbnm*, that, for the polar state, has to be considered as a high-symmetry approximant of a noncentrosymmetric structure. The corresponding structural distortions of *Pbnm* are, in fact, too small to be detected by powder-diffraction method. Nevertheless, this space group allows us to follow the average structural features associated with the magnetoelastic coupling across the magnetic phase transitions, as it will be further described. Table I presents the reliability factors obtained from the final refinement of the atomic positions, for the compositions $x=0$, 0.2, and 0.3, at two different temperatures.

B. Temperature dependence of the lattice parameters

The temperature dependence of a, b, and c lattice parameters, and the unit-cell volume is shown in Figs. 3(a)–3(d), for $x=0$, 0.2, 0.3, and 0.4, respectively. As expected, all parameters decrease monotonously as the temperature decreases toward T_N. The temperature behavior of each lattice parameter above T_N was analyzed in the framework of the Debye thermal-expansion equation, according to[38]

$$\ell(T) = \ell_o + L_a U\left(\frac{\theta_D}{T}\right), \tag{1}$$

where the Debye function is defined as

$$U\left(\frac{\theta_D}{T}\right) = 9RT\left(\frac{T}{\theta_D}\right)^3 \int_0^{\theta_D/T} \frac{x^3}{e^x - 1} dx. \tag{2}$$

Here, ℓ is the lattice parameter, ℓ_o the lattice parameter at $T=0$ K, U stays for the average thermal energy, L_a is a proportionality constant, θ_D denotes the Debye temperature, and R is the gas constant. Within the approximation used in this model, the thermal-expansion coefficient is proportional to the specific heat C_v, and, consequently, the lattice parameter turns out to be directly proportional to the average thermal energy U, just as in Eq. (1). The smooth curves in Fig. 3 are the best fits of Eq. (1) to the experimental data, above the Néel temperature. All data recorded above T_N are well described by Eq. (1). Although the lattice parameters are all of the same order of magnitude, their mean thermal-expansion coefficients ($\langle\alpha\rangle$) depend on both direction and concentration. The coefficient $\langle\alpha\rangle$ was calculated above T_N, and the corresponding values are listed in Table II. The anisotropic character of the samples is again reflected in the differences of the mean values of the thermal expansion. Among the three crystallographic directions, the mean value of the thermal expansion is systematically smaller along the b direction than the other two, which exhibit quite similar values.

TABLE I. Reliability factors obtained from the final refinement of the atomic positions, for the compositions $x=0$, 0.2, and 0.3, at 35 and 50 K.

	30 K				50 K			
x	R_p	R_{wp}	R_B	R_f	R_p	R_{wp}	R_B	R_f
0	3.66	4.86	3.67	2.22	3.68	4.78	3.86	2.50
0.2	1.68	2.54	1.93	1.40	1.78	2.58	2.23	1.58
0.3	1.81	2.60	2.89	1.93	1.62	2.25	2.35	1.60

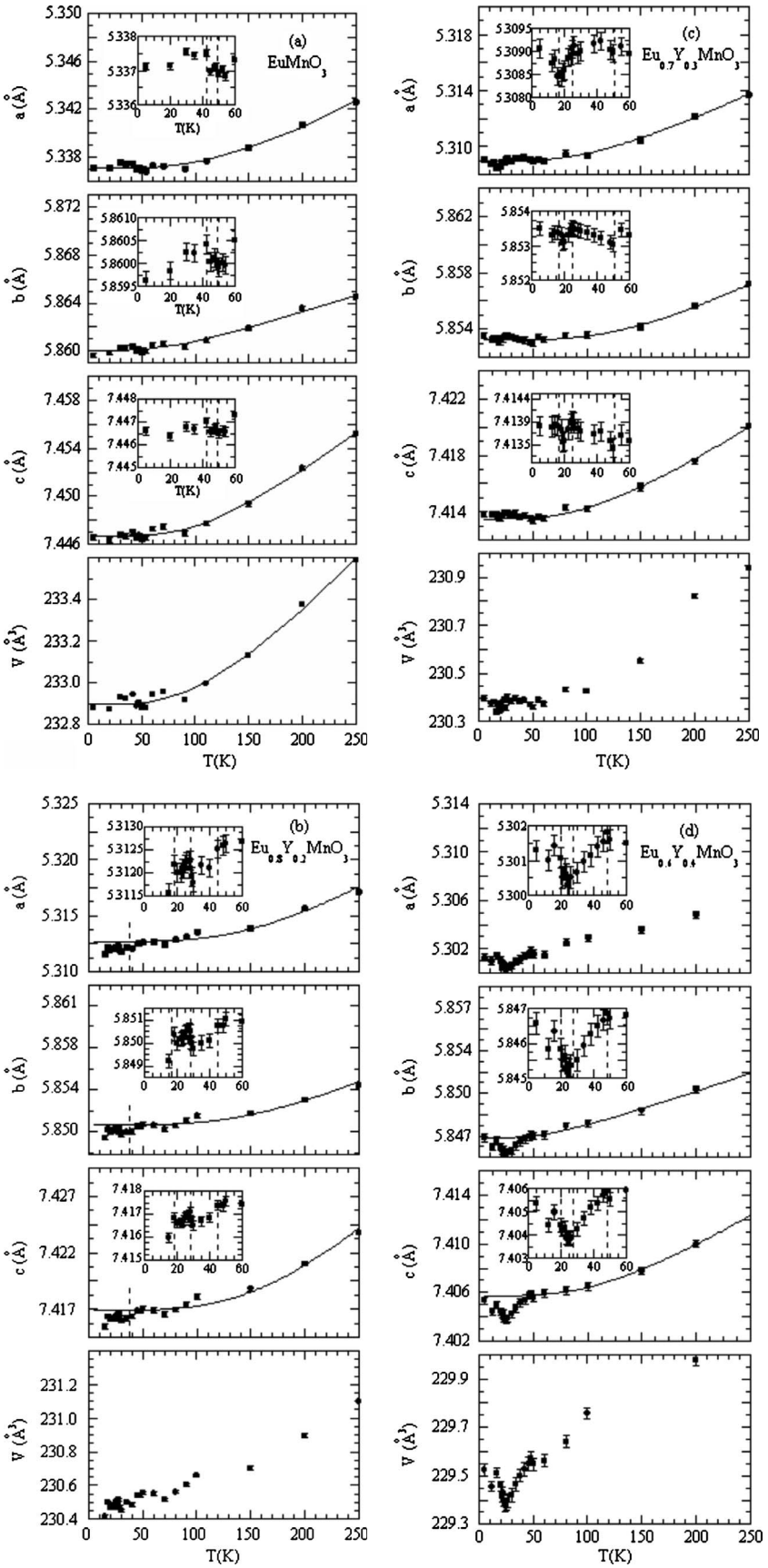

FIG. 3. Temperature dependence of a, b, and c lattice parameters and unit-cell volume, for (a) $x=0$, (b) 0.2, (c) 0.3, and (d) 0.4. The solid lines represent the best fits of Eq. (1) to the experimental data above 100 K. Insets: expanded view of the temperature dependence of the lattice parameters, in the temperature range from 5 to 60 K.

TABLE II. Mean thermal-expansion coefficients ($\langle\alpha\rangle$) along the three crystallographic directions, calculated above T_N, for compositions $x=0$, 0.2, 0.3, and 0.4, respectively.

x	0			0.2			0.3			0.4		
Parameter	a	b	c	a	b	c	a	b	c	a	b	c
$\langle\alpha\rangle\times10^{-6}$ K^{-1}	5.2	2.6	5.8	5.3	3.8	5.7	4.5	3.4	4.4	4.1	3.8	4.2

Significant deviations from the high-temperature Debye behavior are observed below T_N, which are correlated with the onset of the incommensurate magnetic ordering. The temperature dependence of the lattice parameters is strongly dependent on x. The magnetic phase sequence, taking place at lower temperatures, is revealed by small but distinct anomalies in the temperature dependence of the lattice parameters [see insets of Figs. 3(a)–3(d)]. As the Y content increases from $x=0.2$ to $x=0.4$, the anomalies of the lattice parameters become larger, attaining for $x=0.4$ variations in about 0.002 Å between T_N and $T_{AFM\text{-}2}$ [see Fig. 3(d)]. For this composition, minimum values of the lattice parameters occur at around $T_{AFM\text{-}2}$, clearly marking the transition from the incommensurate antiferromagnetic order to the *bc*-cycloidal magnetic structure.

The anomalies observed in the temperature dependence of the lattice parameters across the magnetic phase transitions confirm the existence of a coupling between spins and lattice, in agreement with the results recently reported in a Raman work on this system.[21] The anomalies observed in the temperature dependence of the lattice parameters are a direct consequence of the atomic displacements, taking place at the onset of a new magnetic arrangement, as will be seen in the following section.

C. MnO_6 deformations and spin-lattice coupling

The temperature dependence of Mn-O1, Mn-O21, and Mn-O22 bond lengths, and the Mn-O1-Mn bond angle is depicted in Fig. 4, for the compositions $x=0.2$, 0.3, and 0.4, respectively. The temperature dependence of both bond lengths and bond angle shows significant x dependence, and their anomalies evidence the magnetic phase sequence at low temperatures for each investigated x value.

In the 10–80 K temperature range, for each particular value of x, the Mn-O21 and Mn-O22 bond lengths exhibit the largest temperature variations, which are similar for both distances and increase with x. The length variation in both Mn-O21 and Mn-O22 bonds is almost the same. For $x=0.2$, the maximum Mn-O2 length variation is about 0.02 Å [see Fig. 4(a)] while, for $x=0.4$, this value is about 0.08 Å [see Fig. 4(c)]. The change in the Mn-O1 bond length ranges from 0.01 Å (for $x=0.2$) to 0.04 Å (for $x=0.4$). In a general way, the temperature dependence of the Mn-O1, Mn-O21, and Mn-O22 bond lengths clearly shows anomalous behavior both at T_N and $T_{AFM\text{-}2}$, revealed either by changes in slope or sudden steps. The variations observed at $T_{AFM\text{-}3}$ are consistent with the transition revealed by other experimental techniques at this temperature.[23,24] A detailed examination of the Mn-O21 and Mn-O22 bond lengths as a function of the temperature shows that, except for $x=0.2$ in the AFM-2 phase, these two bonds behave almost oppositely; i.e., while one bond length increases, the other one decreases. Strikingly, the difference between the Mn-O21 and Mn-O22 bond lengths increases with increasing x. The larger difference between the Mn-O21 and Mn-O22 bond lengths occurs for $x=0.4$ at $T_{AFM\text{-}2}$.

The temperature dependence of the tilt angle Mn-O1-Mn also exhibits strong x dependence. For $x=0.2$, the Mn-O1-Mn bond angle as a function of the temperature decreases as the temperature decreases toward $T_{AFM\text{-}2}$, and it shows a clear change in slope at T_N. Below $T_{AFM\text{-}2}$, the Mn-

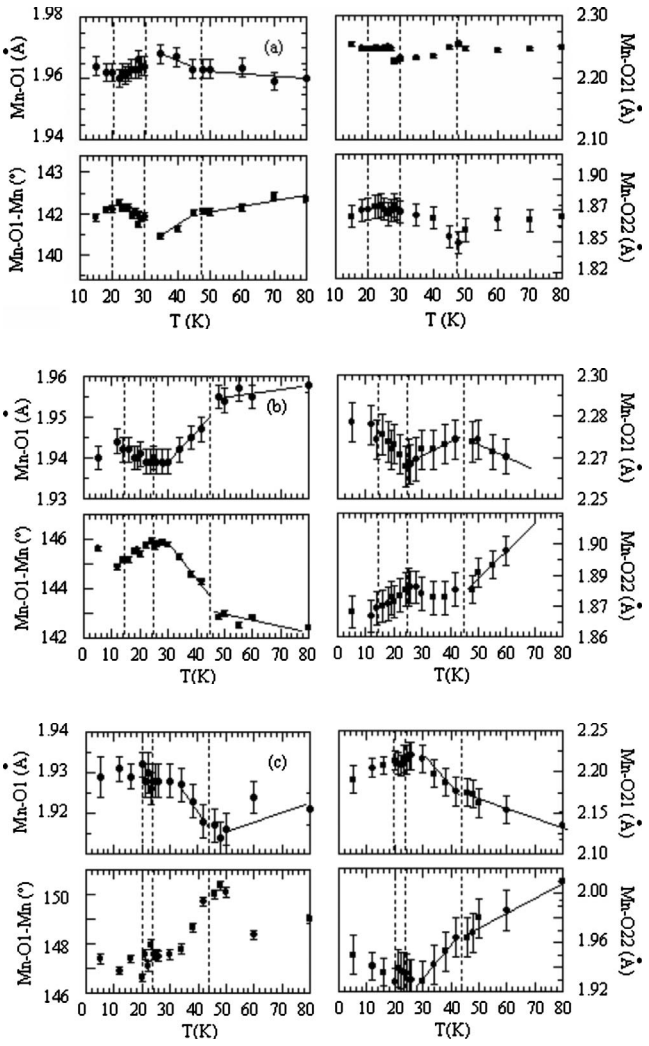

FIG. 4. Temperature dependence of the Mn-O1, Mn-O21, and Mn-O22 bond lengths, and Mn-O1-Mn bond angle of (a) $Eu_{0.8}Y_{0.2}MnO_3$, (b) $Eu_{0.7}Y_{0.3}MnO_3$, and (c) $Eu_{0.6}Y_{0.4}MnO_3$. The vertical dashed lines mark the critical temperatures.

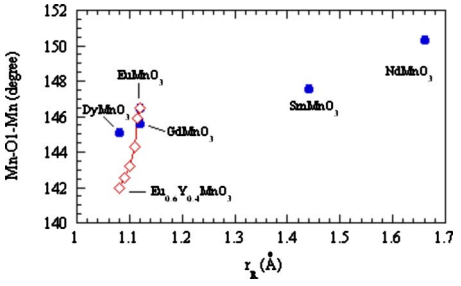

FIG. 5. (Color online) Mn-O1-Mn bond angle as a function of the ionic radius of the A-site ion, for the $RMnO_3$, with R=Nd, Sm, Eu, Gd, and Dy (closed circles), and for $Eu_{0.8}Y_{0.2}MnO_3$ (open squares).

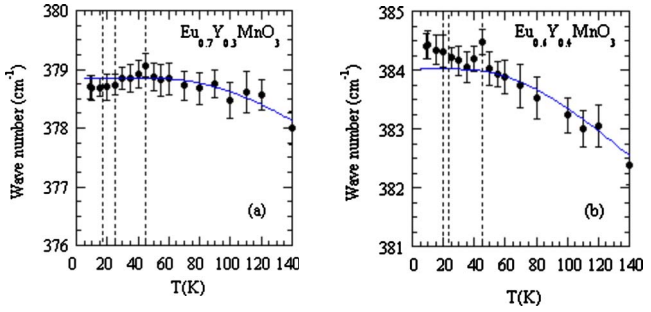

FIG. 6. (Color online) Temperature dependence of the eigenfrequency of the tilt mode of (a) $Eu_{0.7}Y_{0.3}MnO_3$ and (b) $Eu_{0.6}Y_{0.4}MnO_3$. The solid lines represent the best fits of the purely anharmonic temperature behavior of the eigenfrequency to the experimental data for $T>100$ K.

O1-Mn bond angle increases and reaches a maximum value at around $T_{AFM\text{-}3}$. Unlikely, for x=0.3, the Mn-O1-Mn bond angle increases as the temperature decreases, showing a maximum at $T_{AFM\text{-}2}$, and changing its slope at T_N. Finally, for x=0.4, a broad anomaly is observed at T_N. In the incommensurate magnetic phase, the Mn-O1-Mn bond angle decreases, reaching an almost constant value at both $T_{AFM\text{-}2}$ and $T_{AFM\text{-}3}$. The amplitude of the Mn-O1-Mn bond angle anomaly also increases with x, in the 5–80 K temperature range, varying from 1.5° for x=0.2 up to 4° for x=0.4, which is a rather large value.

The aforementioned changes in both bond lengths and bond angle of the MnO_6 octahedra across the magnetic phase-transition temperatures, clearly evidence the existence of a strong coupling between the magnetic order and the lattice.

We should highlight the importance of this result as it definitely confirms assumptions forwarded in previously published works carried out in orthorhombically distorted rare-earth maganites.[8,22–24,32,35] What makes them a very interesting set of materials is the fact that they share a common $GdFeO_3$—distortion, where the tilt angle of the MnO_6 octahedra becomes larger when the rare-earth radius decreases. This behavior is illustrated in Fig. 5 for several undoped rare-earth manganites and the $Eu_{1-x}Y_xMnO_3$ doped system. As it can be seen from Fig. 5, for undoped rare-earth manganites, as the ionic radius decreases, the Mn-O1-Mn bond angle decreases almost linearly. However, for the $Eu_{1-x}Y_xMnO_3$ system, a significant deviation from the linear behavior observed for undoped manganites is detected. It is worth noting that a much steeper slope is observed for the $Eu_{1-x}Y_xMnO_3$ system. Since the slope of the Mn-O1-Mn bond angle as a function of x scales with the degree of competition between both the NN ferromagnetic and the NNN antiferromagnetic exchanges in the basal ab plane, its phase diagram has then to exhibit very unique features, which distinguish the $Eu_{1-x}Y_xMnO_3$ system from the others. Such features are apparent out from experimentally mapped phase diagrams.[22–24,32] The phase diagram of $Eu_{1-x}Y_xMnO_3$ has also been theoretically studied by several authors,[8,9,12,14,39,40] who assumed that the $GdFeO_3$ distortion induces and enhances the NNN antiferromagnetic against the NN ferromagnetic exchanges. Though the Hamiltonian model used can fairly reproduce the experimental (x,T) phase diagram,[39,40] it is unable to describe the data shown in Fig. 4, as no term involving the coupling between the spins and the elastic tensor components has been considered.

The aforementioned MnO_6 distortions of orthorhombic $Eu_{1-x}Y_xMnO_3$ compounds clearly evidence the interplay between spins and lattice, yielding a large magnetoelastic coupling, which actually manifests itself by anomalies in the temperature behavior of the lattice vibrations. The existence of spin-phonon coupling has been evidenced from the anomalous behavior of the eigenfrequency of the symmetric stretching molecular mode associated with the MnO_6 octahedra.[21] However, in order to ascertained the actual effect of the spin ordering on the crystal lattice, we have studied the temperature behavior of the lattice mode associated with the rotational A_g mode of the MnO_6 octahedra, which scales directly with the Mn-O1-Mn bond angle, being the main order parameter.[21] Figure 6 shows the eigenfrequency of the rotational A_g mode of the MnO_6 octahedra as a function of temperature for the particular concentrations x=0.3 and 0.4, respectively. The solid lines represent the best fits of the purely anharmonic temperature behavior of the eigenfrequency to the experimental data for $T>100$ K.[21,41] For x=0.3 [see Fig. 6(a)], a faint anomaly at T_N is apparent, and a negative shift of the eigenfrequency from the high-temperature anharmonic behavior is observed below $T_{AFM\text{-}2}$. For x=0.4 [see Fig. 6(b)], well-defined anomalies at T_N and a positive shift from the high-temperature anharmonic behavior are observed at T_N and $T_{AFM\text{-}2}$, respectively. The negative (positive) shifts of the eigenfrequency regarding the temperature anharmonic behavior have been interpreted as depending on the relative strength between the ferromagnetic and antiferromagnetic exchange interactions, associated with the eigenmode being considered.[21] The above-referred shifts are in good agreement with the weak ferromagnetic character of the $Eu_{0.7}Y_{0.3}MnO_3$, and with the antiferromagnetic character of $Eu_{0.6}Y_{0.4}MnO_3$. The temperature dependence of the eigenfrequency of the lattice mode provides a clear evidence for the significant role played by the spin-phonon coupling mechanism in these materials.

V. CONCLUSIONS

This work provides a detailed experimental study of crystal structure of the orthorhombic $Eu_{1-x}Y_xMnO_3$, with x=0,

0.2, 0.3, and 0.4, across the magnetic phase transitions occurring at low temperatures. This study evidences the existence of a marked magnetoelastic coupling revealed by anomalies observed in lattice parameters at the magnetic phase transitions, also apparent from the anomalous changes in both Mn-O bond lengths and Mn-O1-Mn bond angle. These variations, which are x dependent, yield significant changes in electronic orbitals hybridization, and consequently, in the exchange interactions between Mn spins. As a consequence, this system exhibits a rich phase diagram with very different spin structures and polar properties, according the yttrium concentration up to $x=0.5$. Signatures of the lattice deformations across the magnetic phase transitions were evidenced by anomalies in the temperature dependence of the lattice mode involving rotations of the MnO_6 octahedra. These anomalies confirm the existence of a notable spin-phonon coupling in these materials.

Our experimental findings evidence that oxygen displacements are actively involved in the stabilization of the magnetic and polar stated; as a consequence a shift of phase boundaries at (x,T) phase diagram is expected through isotopic substitution.

ACKNOWLEDGMENTS

This work was supported by Fundação para a Ciência e Tecnologia, through the Project PTDC/CTM/67575/2006, and by Programme Alban.

*jamoreir@fc.up.pt

[1] W. Eerenstein, N. D. Mathur, and J. F. Scott, Nature (London) **442**, 759 (2006).
[2] C.-W. Nan, M. I. Bichurin, S. Dong, and D. Viehland, J. Appl. Phys. **103**, 031101 (2008).
[3] J. Kreisel, B. Noheda, and B. Dkhil, Phase Transitions **82**, 633 (2009).
[4] A. Loidl, H. V. Loehneysen, and G. M. Kalvius, J. Phys.: Condens. Matter **20**, 430301 (2008).
[5] H. Béa, M. Bibes, A. Barthélémy, K. Bouzehougne, E. Jacquet, A. Khodan, and J.-P. Contour, S. Fusil, F. Wyczisk, A. Forget, D. Lebeugle, D. Colson, and M. Viret, Appl. Phys. Lett. **87**, 072508 (2005).
[6] M. Bibes and A. Barthélémy, IEEE Trans. Electron Devices **54**, 1003 (2007).
[7] T. Goto, T. Kimura, G. Lawes, A. P. Ramirez, and Y. Tokura, Phys. Rev. Lett. **92**, 257201 (2004).
[8] T. Kimura, S. Ishihara, H. Shintani, T. Arima, K. T. Takahashi, K. Ishizaka, and Y. Tokura, Phys. Rev. B **68**, 060403 (2003).
[9] T. Goto, Y. Yamasaki, H. Watanabe, T. Kimura, and Y. Tokura, Phys. Rev. B **72**, 220403 (2005).
[10] R. Valdés Aguilar, M. Mostovoy, A. B. Sushkov, C. L. Zhang, Y. J. Choi, S.-W. Cheong, and H. D. Drew, Phys. Rev. Lett. **102**, 047203 (2009).
[11] H. Katsura, N. Nagaosa, and A. V. Balatsky, Phys. Rev. Lett. **95**, 057205 (2005).
[12] I. A. Sergienko and E. Dagotto, Phys. Rev. B **73**, 094434 (2006).
[13] T. Kimura, G. Lawes, T. Goto, Y. Tokura, and A. P. Ramirez, Phys. Rev. B **71**, 224425 (2005).
[14] S. Dong, R. Yu, S. Yunoki, J.-M. Liu, and E. Dagotto, Phys. Rev. B **78**, 155121 (2008).
[15] I. Kagomiya, S. Matsumoto, K. Kohn, Y. Fukuda, T. Shoubu, H. Kimura, Y. Noda, and N. Ikeda, Ferroelectrics **286**, 167 (2003).
[16] C. Wang, G.-C. Guo, and L. He, Phys. Rev. Lett. **99**, 177202 (2007).
[17] C. Wang, G.-C. Guo, and L. He, Phys. Rev. B **77**, 134113 (2008).
[18] G. Giovannetti and J. van den Brink, Phys. Rev. Lett. **100**, 227603 (2008).
[19] S. Lee, A. Pigorov, M. Kang, K.-H. Jang, M. Yonemura, T. Kamiyama, S.-W. Cheong, F. Gozzo, N. Shin, H. Kimura, Y. Noda, and J.-G. Park, Nature (London) **451**, 805 (2008).
[20] W. S. Ferreira, J. Agostinho Moreira, A. Almeida, M. R. Chaves, J. P. Araújo, J. B. Oliveira, J. M. Machado Da Silva, M. A. Sá, T. M. Menconça, P. Simeão Carvalho, J. Kreisel, J. L. Ribeiro, L. G. Vieira, P. B. Tavares, and S. Mendonça, Phys. Rev. B **79**, 054303 (2009).
[21] J. Agostinho Moreira, A. Almeida, W. S. Ferreira, J. E. Araújo, A. M. Pereira, M. R. Chaves, J. Kreisel, S. M. F. Vilela, and P. B. Tavares, Phys. Rev. B **81**, 054447 (2010).
[22] V. Yu. Ivanov, A. A. Mukhin, V. D. Travkin, A. S. Prokhorov, Yu. F. Popov, A. M. Kadomtseva, G. P. Vorob'ev, K. I. Kamilov, and A. M. Balbashov, Phys. Status Solidi B **243**, 107 (2006).
[23] J. Hemberger, F. Schrettle, A. Pimenov, P. Lunkenheimer, V. Yu. Ivanov, A. A. Mukhin, A. M. Balbashov, and A. Loidl, Phys. Rev. B **75**, 035118 (2007).
[24] Y. Yamasaki, S. Miyasaka, T. Goto, H. Sagayama, T. Arima, and Y. Tokura, Phys. Rev. B **76**, 184418 (2007).
[25] A. Pimenov, A. Loidl, A. A. Mukhin, V. D. Travkin, V. Yu. Ivanov, and A. M. Balbashov, Phys. Rev. B **77**, 014438 (2008).
[26] R. Valdés Aguilar, A. B. Sushkov, C. L. Zhang, Y. J. Choi, S.-W. Cheong, and H. D. Drew, Phys. Rev. B **76**, 060404(R) (2007).
[27] A. Pimenov, A. M. Shuvaev, A. A. Mukhin, and A. Loidl, J. Phys.: Condens. Matter **20**, 434209 (2008).
[28] Y. Takahashi, Y. Yamasaki, N. Kida, Y. Kaneko, T. Arima, R. Shimano, and Y. Tokura, Phys. Rev. B **79**, 214431 (2009).
[29] M. Mochizuki and N. Furukawa, J. Phys. Soc. Jpn. **78**, 053704 (2009).
[30] M. Tokunaga, Y. Yamasaki, Y. Onose, M. Mochizuki, N. Furukawa, and Y. Tokura, Phys. Rev. Lett. **103**, 187202 (2009).
[31] H. Murakawa, Y. Onose, F. Kagawa, S. Ishiwata, Y. Kaneko, and Y. Tokura, Phys. Rev. Lett. **101**, 197207 (2008).
[32] J. Agostinho Moreira, A. Almeida, W. S. Ferreira, M. R. Chaves, J. P. Araújo, A. M. Pereira, S. M. F. Vilela, and P. B. Tavares, J. Phys.: Condens. Matter **22**, 125901 (2010).
[33] J. Agostinho Moreira, A. Almeida, W. S. Ferreira, M. R. Chaves, S. M. F. Vilela, P. B. Tavares, B. Kundys, R. Ranjith, and W. Prellier, J. Appl. Phys. **107**, 024108 (2010).
[34] J. A. Alonso, M. J. Martínez-Lope, M. T. Casais, and M. T. Fernández-Díaz, Inorg. Chem. **39**, 917 (2000).
[35] J. Agostinho Moreira, A. Almeida, W. S. Ferreira, M. R. Chaves, B. Kundys, R. Ranjith, W. Prellier, S. M. F. Vilela, and P. B.

Tavares, J. Phys.: Condens. Matter **21**, 446002 (2009).
[36] A. Hammerslev, ESRF Internal Report No. EXP/AH/95-01, 1995 (inpublished).
[37] J. Rodriguez-Carvajal, Physica B: Condensed Matter **192**, 55 (1993).
[38] C. Kittel, *Introduction à la Physique d'État Solide*, 3rd ed. (Dunod, Paris, 1972).
[39] M. Mochizuki and N. Furukawa, Phys. Rev. B **80**, 134416 (2009).
[40] M. Mochizuki, N. Furukawa, and N. Nagaosa, Phys. Rev. Lett. **104**, 177206 (2010).
[41] M. Balkanski, R. F. Wallis, and E. Haro, Phys. Rev. B **28**, 1928 (1983).